

# Electric and magnetic response of hot QCD matter

T. Steinert\* and W. Cassing

*Institut für Theoretische Physik, Universität Giessen, 35392 Giessen, Germany*

(Dated: October 31, 2018)

We study the electric conductivity as well as the magnetic response of hot QCD matter at various temperatures  $T$  and chemical potentials  $\mu_q$  within the off-shell Parton-Hadron-String Dynamics (PHSD) transport approach for interacting partonic systems in a finite box with periodic boundary conditions. The response of the strongly-interacting system in equilibrium to an external electric field defines the electric conductivity  $\sigma_0$  whereas the response to a moderate external magnetic field defines the induced diamagnetic moment  $\mu_L(T, \mu_q)$  as well as the spin susceptibility  $\chi_S(T, \mu_q)$ . We find a sizeable temperature dependence of the dimensionless ratio  $\sigma_0/T$  well in line with calculations in a relaxation time approach for  $T_c < T < 2.5T_c$  as well as an increase of  $\sigma_0$  with  $\mu_q^2/T^2$ . Furthermore, the frequency dependence of the electric conductivity  $\sigma(\Omega)$  shows a simple functional form well in line with results from the Dynamical QuasiParticle Model (DQPM). The spin susceptibility  $\chi_S(T, \mu_q)$  is found to increase with temperature  $T$  and to rise  $\sim \mu_q^2/T^2$ , too. The actual values for the magnetic response of the QGP in the temperature range below 250 MeV show that the QGP should respond diamagnetically in actual ultra-relativistic heavy-ion collisions since the maximal magnetic fields created in these collisions are smaller than  $B_c(T)$  which defines a boundary between diamagnetism and paramagnetism.

PACS: 12.38.Mh, 11.30.Rd, 25.75.-q, 13.40.-f

## I. INTRODUCTION

The phase diagram of strongly interacting hadronic/partonic matter has been a subject of primary interest in the physics community for decades. At vanishing (or low) chemical potentials lattice QCD (lQCD) calculations have provided reliable results on the equation of state [1, 2] and given a glance at the transport properties in particular in the partonic phase. On the other hand high energy heavy-ion reactions are studied experimentally and theoretically to obtain information about the properties of nuclear matter under the extreme conditions of high baryon density and/or temperature. Ultra-relativistic heavy-ion collisions at the Relativistic Heavy-Ion Collider (RHIC) and the Large Hadron Collider (LHC) at CERN have produced a new state of matter, the strongly interacting quark-gluon plasma (sQGP), for a couple of fm/c in volumes up to a few  $10^3 \text{ fm}^3$  in central reactions. The produced QGP shows features of a strongly-interacting fluid unlike a weakly-interacting parton gas [3] as had been expected from perturbative QCD (pQCD). Large values of the observed azimuthal asymmetry of charged particles in momentum space [4–8], i.e. the elliptic flow  $v_2$  could quantitatively be well described by ideal hydrodynamics up to transverse momenta of the order of 1.5 GeV/c [9–14]. Recent studies of ‘QCD matter’ in equilibrium – using lattice QCD calculations [15, 16] or partonic transport models in a finite box with periodic boundary conditions [17, 18] – have demonstrated that the ratio of the shear viscosity to entropy density  $\eta/s$  should

have a minimum close to the critical temperature  $T_c$ , similar to atomic and molecular systems [19]. On the other hand, the ratio of the bulk viscosity to the entropy density  $\zeta/s$  should have a maximum close to  $T_c$  [18] or might even diverge at  $T_c$  [20–24]. Indeed, the minimum of  $\eta/s$  at  $T_c \approx 160 \text{ MeV}$  is close to the lower bound of a perfect fluid with  $\eta/s = 1/(4\pi)$  [25] for infinitely coupled supersymmetric Yang-Mills gauge theory (based on the AdS/CFT duality conjecture). This suggests the ‘hot QCD matter’ to be the ‘most perfect fluid’ [26–28]. On the empirical side, relativistic viscous hydrodynamic calculations (using the Israel-Stewart framework) also require a very small  $\eta/s$  of 0.08 – 0.24 in order to reproduce the RHIC elliptic flow  $v_2$  data [29–32]; these phenomenological findings thus are in accord with the theoretical studies for  $\eta/s$  in Refs. [18, 33, 34].

Whereas shear and bulk viscosities of hot QCD matter at finite temperature  $T$  presently are roughly known, the electric conductivity  $\sigma_0$  is a further macroscopic quantity of interest [35, 36] since it controls the electromagnetic emissivity of the plasma. First results from lattice calculations on the electromagnetic correlator have provided results that varied by more than an order of magnitude [37–41]. Furthermore, the conductivity dependence on the temperature  $T$  (at  $T > T_c$ ) is widely unknown, too. The electric conductivity  $\sigma_0$  is also important for the creation of electromagnetic fields in ultra-relativistic nucleus-nucleus collisions from partonic degrees-of-freedom, since  $\sigma_0$  specifies the imaginary part of the electromagnetic (retarded) propagator and leads to an exponential decay of the propagator in time  $\sim \exp(-\sigma_0(t-t')/(\hbar c))$  [42].

Apart from the electric conductivity the magnetic response of the QGP (or strong vacuum) to external magnetic fields  $\mathbf{B}$  has also been of current interest from the

---

\*Electronic address: Thorsten.Steinert@theo.physik.uni-giessen.de

experimental side [43–48] as well as from lattice QCD [49–52]. Strong magnetic fields are created in peripheral relativistic nucleus-nucleus collisions by the charges of the spectator protons during the passage time of the nuclei [48, 53, 54] and at the top RHIC energy of  $\sqrt{s_{NN}} = 200$  GeV magnetic fields of order  $eB \approx 5m_\pi^2$  can be reached. This has led to the suggestion of a charge separation effect due to the Chiral-Magnetic-Effect (CME) in these reactions [43–48]. On the other side lQCD has been focusing on the magnetic catalysis of the chiral  $\langle q\bar{q} \rangle$  condensate at very strong  $\mathbf{B}$  fields at low temperature and the inverse magnetic catalysis of the chiral condensate at temperatures close the critical temperature indicating a decrease of  $T_c$  for high magnetic fields. Note, however, that these studies involve time-independent magnetic fields that are significantly higher than those achieved in peripheral nucleus-nucleus collisions for very short times where an equilibrated QGP might not have been established. Nevertheless, a sufficient knowledge of the electric and magnetic response of the QGP (in equilibrium) to external electromagnetic fields is mandatory to explore a possible generation of the Chiral-Magnetic-Effect in predominantly peripheral heavy-ion reactions [43–48] and to determine the photon production from the QGP in heavy-ion collisions at different centralities and bombarding energies [55–57].

In this work we extend our previous studies on the electric conductivity  $\sigma_0(T)$  [58, 59] for ‘infinite parton matter’ also to finite quark chemical potential  $\mu_q$  employing the Parton-Hadron-String Dynamics (PHSD) transport approach [60], which is based on generalized transport equations derived from the off-shell Kadanoff-Baym equations [61, 62] for Green’s functions in phase-space representation (beyond the quasiparticle approximation). This approach describes the full evolution of a relativistic heavy-ion collision from the initial hard scatterings and string formation through the dynamical deconfinement phase transition to the strongly-interacting quark-gluon plasma (sQGP) as well as hadronization and the subsequent interactions in the expanding hadronic phase. In the hadronic sector PHSD is equivalent to the Hadron-String-Dynamics (HSD) transport approach [63–66] – a covariant extension of the Boltzmann-Uehling-Uhlenbeck (BUU) approach [67] – that has been used for the description of  $pA$  and  $AA$  collisions from lower Schwerionen-Synchrotron (SIS) to RHIC energies in the past. On the other hand, the partonic dynamics in PHSD is based on the Dynamical Quasi-Particle Model (DQPM) [68–70], which describes QCD properties in terms of single-particle Green’s functions (in the sense of a two-particle irreducible (2PI) approach) and reproduces lattice QCD results – including the partonic equation of state – in thermodynamic equilibrium. For further details on the PHSD off-shell transport approach and hadronization we refer the reader to Refs. [17, 60, 71, 72].

The layout of our study is as follows: In Section II we concentrate on calculating the electric conductivity for ‘infinite’ QCD matter also at finite quark chemical

potential  $\mu_q$  and provide simple parametrizations for the dependence of  $\sigma_0$  on  $\mu_q$ . Furthermore, we calculate the frequency dependence  $\sigma(\Omega)$  for periodic external fields and compare the results with those from the Dynamical QuasiParticle Model (DQPM). In Section III we compute the diamagnetic and paramagnetic contributions to the magnetization  $M$  of the plasma as a function of temperature  $T$  and  $\mu_q$  and compare to the experimental situation at RHIC. A summary and discussion of results is presented in Section IV.

## II. ELECTRIC CONDUCTIVITY

We briefly recall the setup of our studies within PHSD. The ‘infinite’ hadronic or QCD matter is simulated within a cubic box with periodic boundary conditions at various values for the energy density (or temperature) and the quark chemical potential  $\mu_q$ . The size of the box is fixed to  $V = 9^3 \text{ fm}^3$  as in the previous investigations [17, 18, 58]. The initialization is done by populating the box with light ( $u, d$ ) and strange ( $s$ ) quarks, antiquarks and gluons slightly out of equilibrium. The system approaches kinetic and chemical equilibrium during its time evolution within PHSD. For more details on the simulation of equilibrated partonic systems using PHSD in the box at finite temperature  $T$  and quark chemical potential  $\mu_q$  we refer the reader to Ref. [17].

We recall that PHSD is an off-shell transport approach that propagates quasi-particles with broad spectral functions. Numerically, the continuous spectral distribution in the mass of a particle (given by its spectral function) is probed by a large number of test-particles with (evolving) masses  $M_j(t)$ . In order to include the effects from an external electric field  $\mathbf{E}$  or magnetic field  $\mathbf{B}$ , the propagation of each charged test-particle  $j$  is performed with the additional Lorentz force in the equation of motion:

$$\frac{d}{dt} \mathbf{p}^j = q_j e (\mathbf{E} + \frac{\mathbf{p}^j}{E^j} \times \mathbf{B}), \quad (1)$$

where  $q_j$  denotes the fractional charge of the test-particle ( $\pm 1/3, \pm 2/3$ ) and  $E^j$  its energy. We recall that the external electric field will lead to an acceleration of positively and negatively charged particles in opposite directions while the particle scatterings/interactions will damp this acceleration and eventually lead to an equilibrium current (cf. Fig. 1 in Ref. [58]). The electric current density  $j_z(t)$  (for an external electric field in  $z$ -direction) is calculated by

$$j_z(t) = \frac{1}{VN} \sum_{k=1}^N \sum_{j=1}^{N_k(t)} e q_j \frac{p_z^j(t)}{M_j(t)}, \quad (2)$$

where  $M_j(t)$  is the mass of the test-particle  $j$  at time  $t$ . The summation in (2) is carried out over  $N$  ensemble members  $k = 1 \dots N$  while  $N_k(t)$  denotes the time-dependent number of ‘physical’ ( $u, d, s$ ) quarks and antiquarks that varies with time  $t$  due to the processes

$q + \bar{q} \leftrightarrow g \leftrightarrow q' + \bar{q}'$  in a single member of the ensemble (run). The number of runs  $N$  is typically taken as a few hundred which gives a current  $j_z(t)$  practically independent on the number of ensemble members  $N$ . We recall that (without external fields) each run of the ensemble is a microcanonical simulation of the dynamics as inherent in the PHSD transport approach which strictly conserves the total four-momentum as well as all discrete conservation laws (e.g. net fermion number for each flavor etc.) [17]. A note of caution has to be given, since due to an external field we deal with an open system with increasing energy density (temperature) in time. Therefore we employ sufficiently small external fields  $eE_z$ , such that the energy increase during the computation time (in each run) stays below 2% and the increase in temperature below 1 MeV.

### A. Constant electric fields

We find that for constant electric fields up to  $eE_z = 50$  MeV/fm a stable electric current  $j_{eq}$  emerges that is  $\sim E_z$  (cf. Ref. [58]). Accordingly, we obtain the conductivity  $\sigma_0(T, \mu_q)$  from the ratio of the stationary current density  $j_{eq}$  and the electric field strength as

$$\frac{\sigma_0(T, \mu_q)}{T} = \frac{j_{eq}(T, \mu_q)}{E_z T}. \quad (3)$$

The results for the dimensionless ratio (3) at  $\mu_q = 0$  (from Ref. [58]) are displayed in Fig. 1 as a function of the scaled temperature  $T/T_c$  in comparison to more recent lattice QCD results from Refs. [37, 40, 41] and suggest a minimum in the ratio  $\sigma_0(T, \mu_q = 0)/T$  close to the critical temperature  $T_c$  followed by an approximate linear rise up to  $2 T_c$  (cf. Ref. [58]). The most recent lQCD results [37, 40, 41] are roughly compatible with the PHSD calculations. Moreover, the lattice data from Ref. [73] give support for the linearity of  $\sigma_0/T$  with temperature above  $T_c$ .

We now focus on the explicit dependence of  $\sigma_0(T, \mu_q)/T$  as a function of the chemical potential  $\mu_q$  which is shown in Fig. 2 for a fixed temperature  $T=200$  MeV. The numerical result can be fitted with a quadratic correction (solid line in Fig. 2)

$$\frac{\sigma_0(T, \mu_q)}{T} = \frac{\sigma_0(T, \mu_q = 0)}{T} (1 + a(T)\mu_q^2). \quad (4)$$

with  $a(T) \approx 11.6 \text{ GeV}^{-2}$  for  $T = 0.2 \text{ GeV}$ . This result comes about as follows: We recall that the electric conductivity of gases, liquids and solid states is described in the relaxation time approach by the Drude formula

$$\sigma_0 = \frac{e^2 n_e \tau}{m_e^*}, \quad (5)$$

where  $n_e$  denotes the density of non-localized charges,  $\tau$  is the relaxation time of the charge carriers in the medium

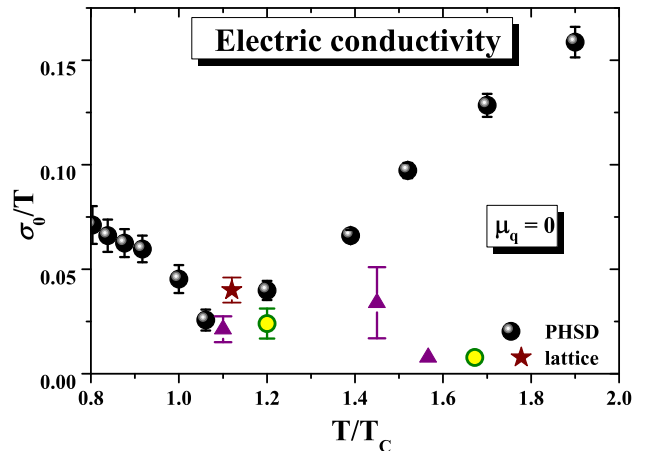


FIG. 1: (Color online) The dimensionless ratio of electric conductivity over temperature  $\sigma_0/T$  (3) as a function of the scaled temperature  $T/T_c$  for  $\mu_q = 0$  in comparison to recent lattice QCD results: triangles - quenched QCD results in the continuum limit with Wilson-Clover fermions and renormalized vector currents [37], star - quenched SU(2) lattice gauge theory [40], open circle - QCD with two dynamical flavors of Wilson-Clover fermions [41]. The PHSD results (full dots) are the same as in Ref. [58].

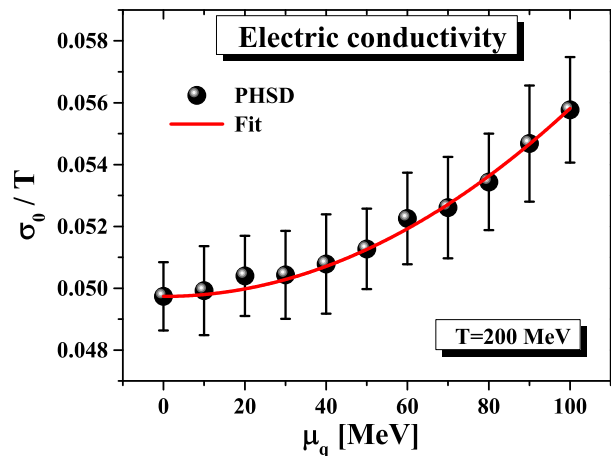


FIG. 2: (Color online) The electric conductivity over temperature  $\sigma_0/T$  as a function of the chemical potential  $\mu_q$  for  $T=200$  MeV from the PHSD calculations (full dots). The error bars indicate the statistical uncertainty for the ratio (3) when performing calculations for different external field strength  $eE_z$  up to 50 MeV/fm.

and  $m_e^*$  their effective mass. This expression can be directly computed for partonic degrees-of-freedom within the DQPM, which was used to match in PHSD the quasi-particles properties to lattice QCD results in equilibrium for the equation-of-state (EoS) as well as various correlators [68–70]. We note that the electromagnetic correlator from lQCD calculations [37] appears to match rather well the back-to-back dilepton rate from PHSD at  $T = 1.45 T_c$  (cf. Fig. 2 in Ref. [74]), which suggests that the results

of our calculations for  $\sigma_0$  - for vanishing invariant mass - should also be close to the IQCD extrapolations from [37].

In the DQPM, the relaxation time for quarks/antiquarks is given by  $\tau = 1/\Gamma_q(T, \mu_q)$ , where  $\Gamma_q(T, \mu_q)$  is the width of the quasiparticle spectral function (cf. [68, 71]). Furthermore, the spectral distribution for the mass of the quasiparticle has a finite pole mass  $M_q(T, \mu_q)$  that is also fixed in the DQPM, as well as the density of  $(u, \bar{u}, d, \bar{d}, s, \bar{s})$  quarks/antiquarks as a function of temperature and chemical potential (cf. Refs. [68, 71]). Thus, we obtain for the dimensionless ratio (3) the expression [58]

$$\frac{\sigma_0(T, \mu_q)}{T} \approx \frac{2}{9} \frac{e^2 n_{q+\bar{q}}(T, \mu_q)}{M_q(T, \mu_q) \Gamma_q(T, \mu_q) T}, \quad (6)$$

where  $n_{q+\bar{q}}(T, \mu_q)$  denotes the total density of quarks and antiquarks and the prefactor  $2/9$  reflects the flavor averaged fractional quark charge squared  $(\sum_f q_f^2)/3$ . As found in our previous study [58] the DQPM results match well with the explicit PHSD calculations in the box for  $\mu_q=0$  since PHSD in equilibrium is a suitable transport realization of the DQPM [17].

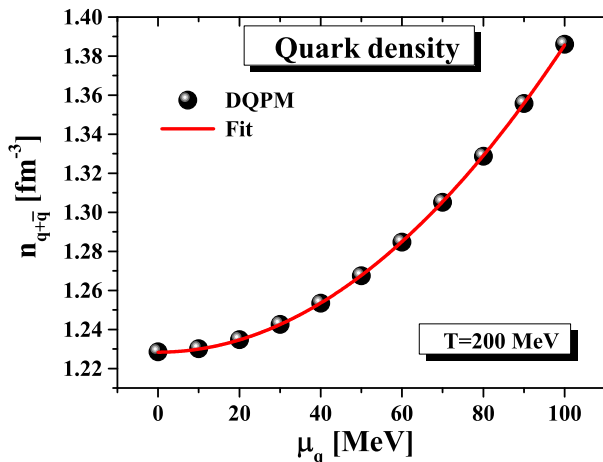


FIG. 3: (Color online) Quark+antiquark density from the DQPM (full dots) as a function of the quark chemical potential  $\mu_q$  for  $T = 200$  MeV. The solid (red) line displays the fit (7) to the DQPM results.

In the DQPM we have  $\Gamma_q(T, \mu_q) \approx \Gamma_q(T, \mu_q = 0)$  and  $M_q(T, \mu_q) \approx M_q(T, \mu_q = 0)$  for  $\mu_q \leq 100$  MeV, however,

$$n_{q+\bar{q}}(T, \mu_q) \approx n_{q+\bar{q}}(T, \mu_q = 0) (1 + a(T) \mu_q^2) \quad (7)$$

with the same coefficient  $a(T)$  as in Eq. (4). This is demonstrated explicitly in Fig. 3 where the actual DQPM results for the quark+antiquark density (full dots) are compared to the fit (7) (solid line).

The temperature dependence of the expansion coefficient  $a(T)$  is found to be  $\sim 1/T^2$  such that the ratio  $\sigma_0/T$  can be approximated by

$$\frac{\sigma_0(T, \mu_q)}{T} \approx \frac{\sigma_0(T, \mu_q = 0)}{T} \left( 1 + c_{\sigma_0} \frac{\mu_q^2}{T^2} \right). \quad (8)$$

In Fig. 4 we display the coefficient  $c_{\sigma_0}$  in the temperature range  $170 \text{ MeV} \leq T \leq 250 \text{ MeV}$  giving  $c_{\sigma_0} \approx 0.46$  as a best fit. This completes our study on the stationary electric conductivity  $\sigma_0$ .

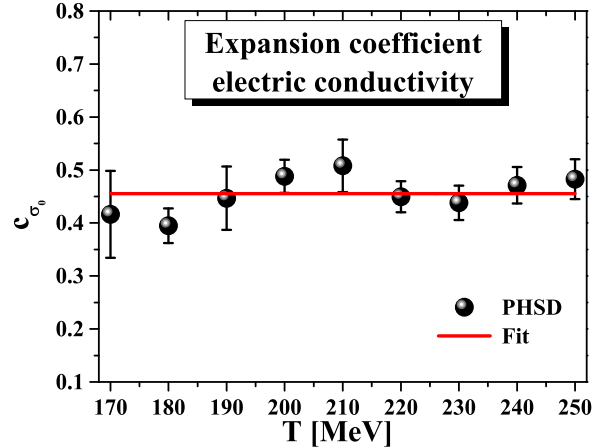


FIG. 4: (Color online) The expansion factor  $c_{\sigma_0}$  in (8) as a function of the temperature  $T$  for  $\mu_q \leq 100$  MeV. The solid line shows the average value in the interval  $170 \text{ MeV} < T < 250 \text{ MeV}$ .

## B. Periodic electric fields

We now extend our study to external periodic fields of frequency  $\Omega$ ,

$$E_z(t) = E_z^0 \sin(\Omega t). \quad (9)$$

In this case the electric current density  $j_z(t)$  does not achieve a constant equilibrium value and also oscillates with the frequency  $\Omega$ . Fig. 5 shows the time-dependence of the current  $j_z(t)$  from PHSD for different frequencies as a function of  $\Omega t$  with their amplitudes normalized to one in comparison to the external electric field  $E_z(t)$  (dotted red line). The current  $j_z(t)$  is seen to be shifted in phase compared to the electric field; the phase shift  $\delta$  increases with the frequency  $\Omega$  up to  $\pi/2$ . The currents in Fig. 5 can be well described by

$$j_z(t) = A(\Omega) j_{eq} \sin(\Omega t - \delta(\Omega)). \quad (10)$$

We find that the amplitude  $A(\Omega)$  decreases with the frequency  $\Omega$  since the current has less time to build up and to follow the external field. This behavior is in line with the complex conductivity  $\sigma(\Omega)$  for oscillating fields,

$$\sigma(\Omega) = \frac{\sigma_0}{1 - i\Omega/\Gamma_q} = \frac{\sigma_0}{1 + \Omega^2/\Gamma_q^2} + i \frac{\sigma_0 \Omega/\Gamma_q}{1 + \Omega^2/\Gamma_q^2}, \quad (11)$$

where  $\Gamma_q$  is the quasi-particle width of the charged particles (quarks and antiquarks). We have computed the current  $j_z(t)$  for  $T = 190$  MeV and  $eE_z^0 = 0.005 \text{ GeV}^2 \approx$

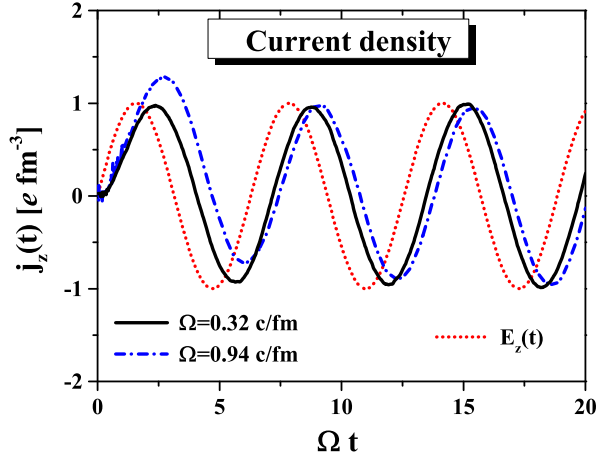


FIG. 5: (Color online) The time-dependent electric current density  $j_z(t)$  for  $\Omega = 0.32$  c/fm (solid black) and  $\Omega = 0.94$  c/fm (dash dotted blue) normalized to the equilibrium amplitude for temperature  $T = 190$  MeV and  $eE_z^0 = 0.005$  GeV<sup>2</sup>  $\approx 25$  MeV/fm. The dotted red line shows the time-dependence of the external electric field  $E_z(t)$ .

25 MeV/fm in the frequency range  $0.02$  c/fm  $< \Omega < 25$  c/fm. Fig. 6 shows the phase shift  $\delta = \arctan(\Omega/\Gamma_q)$  and Fig. 7 the amplitude  $A(\Omega) = 1/\sqrt{1 + \Omega^2/\Gamma_q^2}$  (full dots). The PHSD results can be easily followed up within the DQPM results (shown by the red lines) which provide again a good description of the microscopic calculations. Since the complex conductivity  $\sigma(\Omega)$  depends only on the width  $\Gamma_q$  and the stationary conductivity  $\sigma_0$  in (11) its actual values for different temperatures  $T$  and finite chemical potential  $\mu_q$  follow directly from our previous results in this Section. Note that for actual electric fields in peripheral Au+Au collisions at the top RHIC energy we have  $\Omega \approx 22$  c/fm such that the electric conductivity  $\sigma(\Omega)$  is suppressed relative to its equilibrium value by more than a factor of 100.

### III. MAGNETIC RESPONSE

In order to explore the magnetic response of the partonic system within PHSD we will assume the magnetic field to be sufficiently small such that terms  $\sim B^2$  can be neglected (see below). Note that this limit does not hold for the strong fields  $eB$  ( $\sim 0.1$ - $1$  GeV<sup>2</sup>  $\approx 0.5$ - $5$  GeV/fm) in actual lattice QCD studies [50–52]. Using

$$(\sigma \mathbf{D})^2 = \mathbf{D}^2 - qe\sigma \cdot \mathbf{B}, \quad \mathbf{D}^2 = (\mathbf{p} - qe\mathbf{A})^2 = \mathbf{p}^2 - qe\mathbf{L} \cdot \mathbf{B} \quad (12)$$

with the Pauli matrices  $\sigma$ , the kinetic momentum  $\mathbf{p}$  and the angular momentum  $\mathbf{L}$  the Dirac equation can be rewritten for 2-component quark and antiquark spinors leading to the Hamiltonian

$$H_{Dirac} = \sqrt{\mathbf{p}^2 + m^2} - qe(\mathbf{L} + \sigma) \cdot \mathbf{B} \quad (13)$$

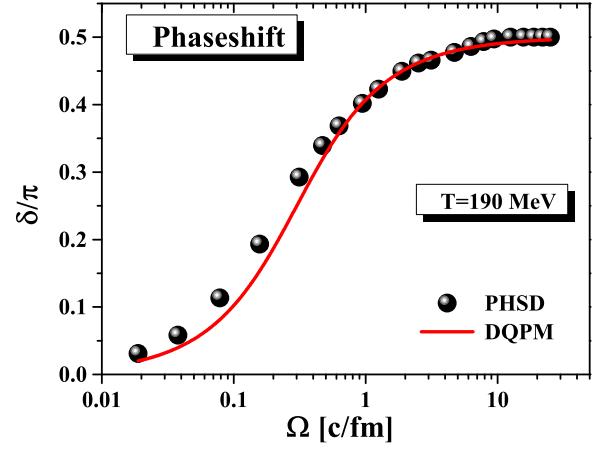


FIG. 6: (Color online) The phase shift  $\delta$  over  $\pi$  as a function of the frequency  $\Omega$  from the PHSD calculations (full dots) for  $T = 190$  MeV. The red line shows the phase shift as expected from the DQPM using (11).

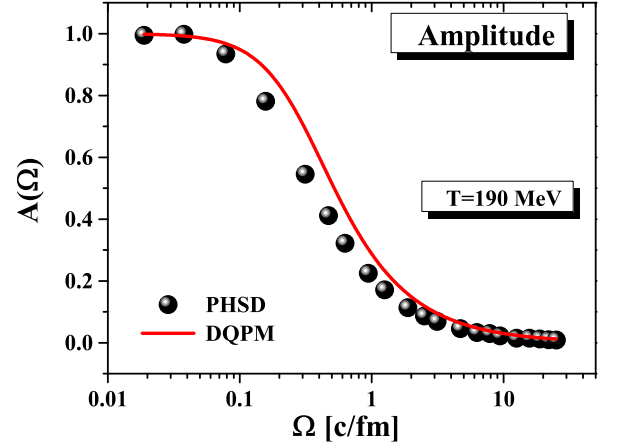


FIG. 7: (Color online) The amplitude  $A(\Omega)$  as a function of the frequency  $\Omega$  from the PHSD calculations (full dots) for  $T = 190$  MeV. The red line shows the expected amplitude within the DQPM.

$$\approx E - \frac{qe}{2E}(\mathbf{L} + \sigma) \cdot \mathbf{B} = E - \frac{qe}{2E}(\mathbf{L} + 2\mathbf{S}) \cdot \mathbf{B}$$

with  $E = \sqrt{\mathbf{p}^2 + m^2}$ . In case of small energies  $E \rightarrow \frac{\mathbf{p}^2}{2m} + m$  this leads to the well known expression for the non-relativistic Pauli equation:

$$H_{Pauli} = \frac{\mathbf{p}^2}{2m} - \frac{qe}{2m}(\mathbf{L} + \sigma) \cdot \mathbf{B}. \quad (14)$$

The change of the energy of the system in the presence of an external magnetic field  $\mathbf{B}$  is determined by the magnetic moment  $\mu$ :

$$\mu = \mu_L + \mu_S = \frac{qe}{2E}(\mathbf{L} + 2\mathbf{S}), \quad (15)$$

which has a contribution from the angular momentum  $\mathbf{L}$  of a particle and from the spin  $\mathbf{S} = \sigma/2$ . In the following

we will investigate both terms separately since they provide contributions to the magnetic moment of opposite sign. In analogy to Sec. II we are dealing with an open system but the increase in the total energy stays below 1%.

### A. Diamagnetic contribution

The induced angular momentum  $\mathbf{L}$  emerges from the Lorentz force (1) on a charged particle due to an external field  $\mathbf{B}$ ,

$$\mathbf{F}_L = \frac{qe}{E}(\mathbf{p} \times \mathbf{B}), \quad (16)$$

and induces a magnetic moment opposite to the direction of the  $\mathbf{B}$ -field since the charged particle spirals around the magnetic field with frequency  $\omega = \frac{qeB}{E} = \frac{p_\perp}{ER}$ , where  $p_\perp$  is the momentum component of the particle perpendicular to the direction of the magnetic field and  $R$  is the radius of the spiral. We obtain alternatively for the angular momentum

$$\mathbf{L} = \frac{Rqe}{|\mathbf{F}_L|E}(\mathbf{p}(\mathbf{p} \cdot \mathbf{B}) - \mathbf{B}p^2), \quad (17)$$

where  $\mathbf{p}(\mathbf{p} \cdot \mathbf{B})$  is the projection of the momentum on the direction of the magnetic field  $\mathbf{e}_B$ . Inserting the expression for the radius  $R$  we get

$$\mathbf{L} = \frac{-p_\perp^3}{|\mathbf{F}_L|E} \text{sign}(q)\mathbf{e}_B. \quad (18)$$

Assuming the magnetic field to be oriented in  $y$ -direction and employing the Lorentz force  $|\mathbf{F}_L| = \frac{|qeB|}{E}p_\perp$  we end up with

$$L_y = \frac{-p_\perp^2}{qeB}. \quad (19)$$

This gives the induced magnetic moment

$$\mu_L = \frac{-p_\perp^2}{2BE}. \quad (20)$$

Since the Lorentz force changes only the direction of  $\mathbf{p}$  and not its magnitude  $|\mathbf{p}|$  the particle energy  $E$  is conserved, too. As a consequence the energy contribution in the Hamiltonian (13) is independent from the magnetic field strength:

$$\Delta E_{mag,L} = -\mu_L B = -\frac{-p_\perp^2}{2BE} B = \frac{p_\perp^2}{2E}. \quad (21)$$

We note that the diamagnetic contribution can not be seen in approaches that calculate the magnetization by differentiation of the thermodynamic potential (e.g. free energy  $F$ ) with respect to the magnetic field  $B$ . In principle, the angular momentum  $\mathbf{L}$  has to be quantized. However, the actual values for  $\mathbf{L}$  (in units of  $\hbar$ ) are  $\gg 1$  for 'small' field strength since  $|\mathbf{L}| \sim 1/(eB)$  such that quantum corrections are subleading in our case.

### B. Paramagnetic contribution

The quark and antiquark spins provide a paramagnetic contribution since the spin precession around the direction of the magnetic field  $\mathbf{B}$  in thermal equilibrium gives a positive magnetic moment  $\mu_S$  since the energy becomes reduced according to Eq. (13). The spin degree-of-freedom is introduced in PHSD in line with the generalized test-particle ansatz [62] for the Wightman function

$$iG^<(X, P, S) = \frac{1}{N} \sum_{k=1}^N \sum_{i=1}^{N_k(t)} \delta^{(3)}(\mathbf{X} - \mathbf{X}_i(t)) \quad (22)$$

$$\times \delta^{(3)}(\mathbf{P} - \mathbf{P}_i(t)) \delta(P_0 - \epsilon_i(t)) \delta^{(2)}(\mathbf{S} - \mathbf{S}_i(t))$$

where  $X$  and  $P$  stand for space-time and four-momentum coordinates, respectively, while  $\mathbf{S}$  denotes the spin degree-of-freedom. In (22) the number of ensemble members (runs) is denoted by  $N$  whereas  $N_k$  is the number of partons in the run  $k = 1 \dots N$  that describe the 'physical' particles in each microcanonical simulation. The spin degree-of-freedom has to be treated in line with quantum mechanics according to the interaction Hamiltonian (13), i.e.

$$\hat{H}_S = -\frac{qe}{2E} \boldsymbol{\sigma} \cdot \mathbf{B}. \quad (23)$$

The spin-wavefunction for a spin 1/2 fermion is taken as a 2-component spinor

$$|\chi\rangle = \begin{pmatrix} \uparrow \\ \downarrow \end{pmatrix} \quad (24)$$

with  $\langle \uparrow | \uparrow \rangle$  denoting the probability for the spin in  $z$ -direction (parallel to the magnetic field) while  $\langle \downarrow | \downarrow \rangle$  stands for the probability for the anti-parallel orientation. We assume the spin-wavefunction to be normalized, i.e.  $\langle \chi | \chi \rangle = \langle \uparrow | \uparrow \rangle + \langle \downarrow | \downarrow \rangle = 1$ . The projection on the coordinate axis  $i$  is provided by

$$S_i = \frac{1}{2} \langle \chi | \sigma_i | \chi \rangle. \quad (25)$$

The time-evolution of the spin projections according to the Hamiltonian (23) can be worked out in a straight forward way using

$$|\chi(t)\rangle = \hat{U}(t, t_0) |\chi(t_0)\rangle = e^{-i\hat{H}_S(t-t_0)} |\chi(t_0)\rangle \quad (26)$$

with

$$\hat{U}(t, t_0) = \mathbb{1}_2 \cos\left(\frac{qe}{2E} B(t-t_0)\right) + i \frac{\boldsymbol{\sigma} \cdot \mathbf{B}}{B} \sin\left(\frac{qe}{2E} B(t-t_0)\right). \quad (27)$$

and Eq. (25). The resulting equations of motion lead to a precession of the spin of a quark/antiquark with frequency  $\omega = qeB/E$  which changes only if the energy of the particle  $E$  changes in a collision or in the inelastic

reaction  $q + \bar{q} \rightarrow g \rightarrow q' + \bar{q}'$ . Since we are using effective interactions, which should be considered as an approximation to the resummed interactions, we can not determine the actual spin of the parton degrees-of-freedom. For this reason we neglect the spin of the gluons and treat the quark spin statistically. In order to describe an equilibration of the spin degree-of-freedom we introduce a spin flip in 1/3 of the elastic collisions, as motivated by nuclear physics, that favors final spin states parallel to the  $\mathbf{B}$ -field. In order to simplify the (time expensive) calculations we introduce the constraint (in equilibrium)

$$\begin{aligned} n_{\uparrow} P_{\uparrow,\downarrow} &= n_{\downarrow} P_{\downarrow,\uparrow} \iff \frac{P_{\uparrow,\downarrow}}{P_{\downarrow,\uparrow}} \\ &= \frac{n_{\downarrow}}{n_{\uparrow}} = \exp(-(E_{\downarrow} - E_{\uparrow})/T) = \exp\left(-\frac{qeB}{ET}\right), \end{aligned} \quad (28)$$

which is introduced explicitly in the transition matrix element squared. Accordingly, in (28)  $P$  denotes the probability for a spin flip and  $n$  the occupation probability for given spin orientation. In practice the probabilities  $P$  are taken as

$$P_{\downarrow,\uparrow} = 1, \quad P_{\uparrow,\downarrow} = \exp\left(-\frac{qeB}{ET}\right) \quad (29)$$

and lead to the proper equilibrium distribution when neglecting the  $q + \bar{q} \leftrightarrow g$  channels. When including these channels we find numerically deviations from the equilibrium distribution by up to 10% since the gluon channels reduce the spin orientation in the direction of the  $\mathbf{B}$ -field, i.e. induce a 'diamagnetic effect'. The actual values of the probabilities (29) are not important for the present study. As long as they fulfill Eq. (28) the equilibrium distribution changes only slightly within statistical error bars. The same holds for the number of collisions with spin flips. Their values are only important for the timescales of the spin equilibration, which, however, we do not address.

The magnetization  $M$  is defined by the spin density of the system as

$$M = \frac{\langle \mu_S \rangle}{V} \approx \chi_S e^2 B, \quad (30)$$

which in case of small magnetic fields  $eB$  - as in our present study - is proportional to the strength of the  $B$ -field thus defining a magnetic susceptibility  $\chi_S$  by

$$\chi_S = \frac{\langle \mu_S \rangle}{e^2 B V}. \quad (31)$$

### C. Numerical results

In order to explore the range of external magnetic fields  $eB$  we can handle reliably within the PHSD calculations for partonic systems we show in Fig. 8 the energy contribution to the magnetic field (21) as a function of  $eB$

for a temperature  $T=190$  MeV. In fact, the calculations for the energy shift due to the magnetic field  $eB$  give constant results for  $eB < 50$  MeV/fm - when discarding the spin degrees-of-freedom - while for stronger fields more significant deviations emerge up to  $\sim 10\%$  for  $eB$  200 MeV/fm. Accordingly, we will restrict to  $eB \leq 100$  MeV/fm ( $\approx 0.01$  GeV<sup>2</sup>) in the following.

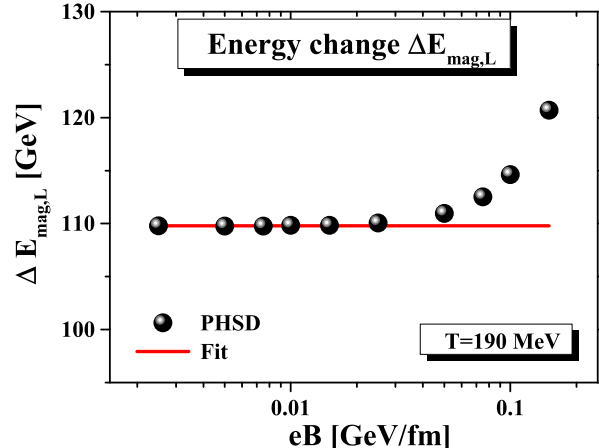


FIG. 8: (Color online) The energy shift due to the magnetic field  $\Delta E_{\text{mag,L}} = -\mu_L B$  in the PHSD calculation (full dots) as a function of the field strength  $eB$  for a temperature of  $T = 190$  MeV at  $\mu_q=0$ . The solid line reflects a constant for small/moderate field strength.

The temperature dependence of  $\Delta E_{\text{mag,L}}$  from the PHSD calculation is shown in Fig. 9 by full dots and can be well fitted in the interval  $170 \text{ MeV} \leq T \leq 250$  MeV by

$$\Delta E_{\text{mag,L}}(T) = 0.3 \cdot (T - 96)^{2.82} [\text{MeV}] \quad (32)$$

where the temperature  $T$  is given in units of MeV. The diamagnetic contribution to the magnetization from the Lorentz force on the quarks and antiquarks then can be readily extracted by dividing  $\Delta E_{\text{mag,L}}(T)$  by the strength of the magnetic field.

As a next step we compute the magnetic susceptibility  $\chi_S$  in the PHSD calculations according to Eq. (31) for different field strength  $eB$  at  $\mu_q = 0$ . We have found the necessary energy for a spin flip to be very small in comparison to the total energy of the quarks ( $< 1\%$ ) and therefore have discarded it in our actual simulations. The results for the susceptibility  $\chi_S$  are displayed in Fig. 10 for  $T=190$  MeV and (within numerical accuracy) show a constant value even up to  $eB=200$  MeV/fm. In this case the numerical accuracy increases with the field strength since the spin-flip probabilities in Eq. (29) differ more significantly for larger magnetic fields. Nevertheless, we have a stable numerical 'window'  $eB$  from 25-50 MeV/fm where the diamagnetic and parametric contributions to the magnetic moment can be calculated with sufficient accuracy. Note that the energy shift due to the param-

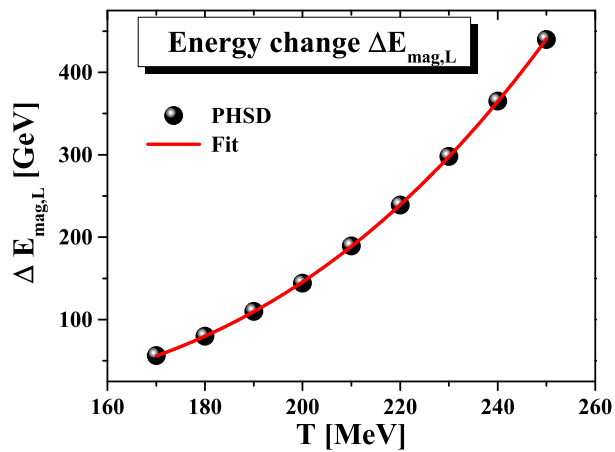


FIG. 9: (Color online) The energy shift due to be magnetic field  $\Delta E_{mag,L} = -\mu_L B$  in the PHSD calculation as a function of the temperature  $T$  for  $\mu_q = 0$ . The numerical uncertainties are smaller than the size of the dots. The solid line shows the fit (32).

agnetic contribution is given by

$$\Delta E_{mag,S} = -\chi_S V (eB)^2 \quad (33)$$

and decreases quadratically with the field strength.

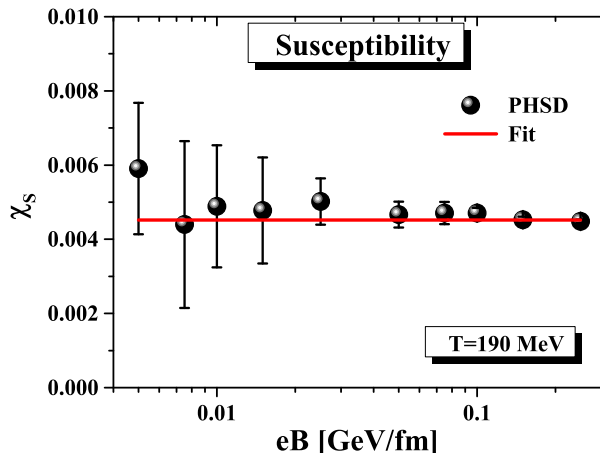


FIG. 10: (Color online) Magnetic susceptibility  $\chi_S$  (31) from PHSD as a function of the external magnetic field  $eB$  for a temperature  $T=190$  MeV at vanishing quark chemical potential  $\mu_q = 0$ .

The temperature dependence of the magnetic susceptibility  $\chi_S(T)$  from PHSD is displayed in Fig. 11 by the full dots and can be fitted as

$$\chi_S(T) = 0.017 - \frac{2.39}{T} \quad (34)$$

with  $T$  given in MeV (in the interval  $170 \text{ MeV} \leq T \leq 250 \text{ MeV}$ ).

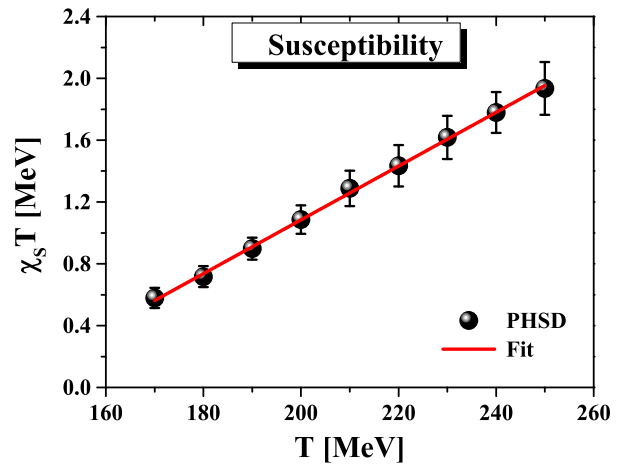


FIG. 11: (Color online) Temperature dependence of the magnetic susceptibility  $\chi_S(T)T$  from PHSD (full dots) in comparison to the fit (34) for  $\mu_q=0$ . The numerical uncertainties are indicated by the errorbars.

The total energy shift due to the both interactions with the magnetic field is given by

$$\Delta E(T, B) = \Delta E_{mag,L}(T) - \chi_S(T) V (eB)^2 \quad (35)$$

and decreases with  $B^2$  at constant temperature  $T$ . At a 'critical' field  $B_c(T)$  the energy shift changes sign, i.e. for

$$B_c(T) = \sqrt{\frac{\Delta E_{mag,L}}{e^2 \chi_S V}} \quad (36)$$

the magnetization changes from diamagnetic to paramagnetic with increasing magnitude of the field  $B$ .

This quantity has a minimum (within PHSD) close to the critical temperature  $T_c \approx 158$  MeV (cf. Fig. 12) with a minimum  $eB_{c,min} \approx 0.4$  GeV<sup>2</sup> (thick solid black line - extrapolated by the dashed line according to the fits performed). For comparison we also show the limiting results when assuming all quark/antiquark spins to be oriented in  $\mathbf{B}$  direction. This line is slightly lower because the coupling to the gluons (in PHSD) reduces the paramagnetic contribution to the magnetization (diamagnetic gluon effect). In the QGP phase the 'critical' field  $B_c$  rises with temperature and separates the diamagnetic (below) from the paramagnetic response (above) of the QGP. Note that the maximal field strength in peripheral Au + Au collisions at the top RHIC energy  $\sqrt{s_{NN}} = 200$  GeV was found to be  $\sim 0.09$  GeV<sup>2</sup> [53] (constant solid line) - during the passage time of the nuclei - which is significantly lower than the 'critical' field in Fig. 12. Accordingly, the response of the QGP in actual heavy-ion experiments should be diamagnetic. However, for the much higher field strength explored in lattice QCD calculations [50–52] for temperatures close to  $T_c$  the response should be paramagnetic.



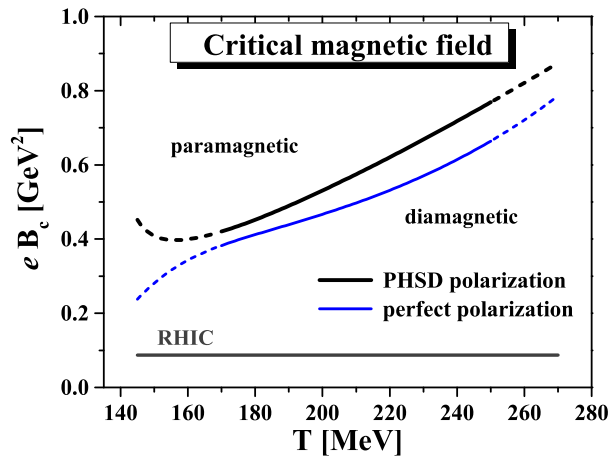


FIG. 12: (Color online) The 'critical' magnetic field (36) as a function of the temperature  $T$  for  $\mu_q = 0$  from the PHSD calculations (thick solid black line). The dashed extensions are based on the extrapolated fits and not explicitly controlled by PHSD calculations. The (lower) thin solid blue line results when assuming all quark/antiquark spins to be oriented in  $\mathbf{B}$  direction. The constant lower line displays the maximum value for the magnetic field strength as found in Ref. [53] at the top RHIC energy.

#### D. Finite quark chemical potential

As in case of the electric conductivity  $\sigma_0(T, \mu_q)$  we can also compute the magnetic response at finite quark chemical potential  $\mu_q$  in PHSD. In analogy to Fig. 2 we find essentially a quadratic dependence on  $\mu_q$  as demonstrated in Fig. 13 for  $\Delta E_{mag,L}(\mu_q)$  at  $T = 200$  MeV. This dependence is also obtained for the magnetic susceptibility  $\chi_S(T, \mu_q)$  (not shown explicitly) although with larger numerical errorbars.

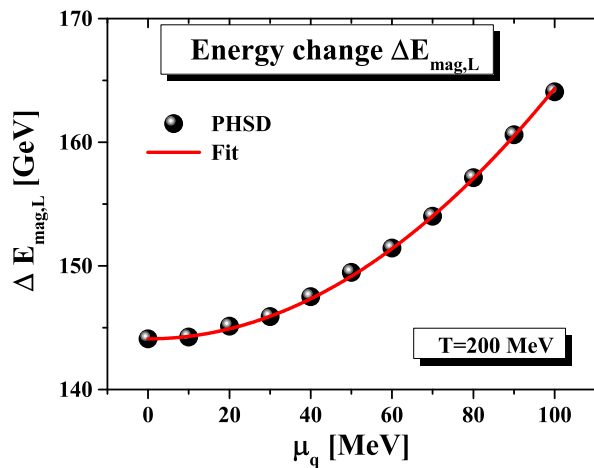


FIG. 13: (Color online) The energy shift  $\Delta E_{mag,L}(T, \mu_q)$  as a function of  $\mu_q$  from PHSD (full dots) in comparison to the fit (37) in  $\mu_q$  (solid line) for  $T = 200$  MeV.

Again we find the temperature dependence of the coefficient to be  $\sim 1/T^2$  such that we get the approximations

$$\Delta E_{mag,L}(T, \mu_q) \approx \Delta E_{mag,L}(T, \mu_q = 0)(1 + c_L \frac{\mu_q^2}{T^2}), \quad (37)$$

$$\chi_S(T, \mu_q) \approx \chi_S(T, \mu_q = 0)(1 + c_S \frac{\mu_q^2}{T^2}).$$

As an example we show the coefficient  $c_L(T)$  in Fig. 14 for temperatures from 190 to 250 MeV. In this temperature interval the expansion coefficient may be well approximated by  $c_L = 0.57$ . Similar statements (with less accuracy) hold for the magnetic susceptibility in (37) which gives  $c_S = 0.49$ . The scaling (37) can be traced back again to the scaling of the quark+antiquark density  $n_{q+\bar{q}}(T, \mu_q)$  in the DQPM.

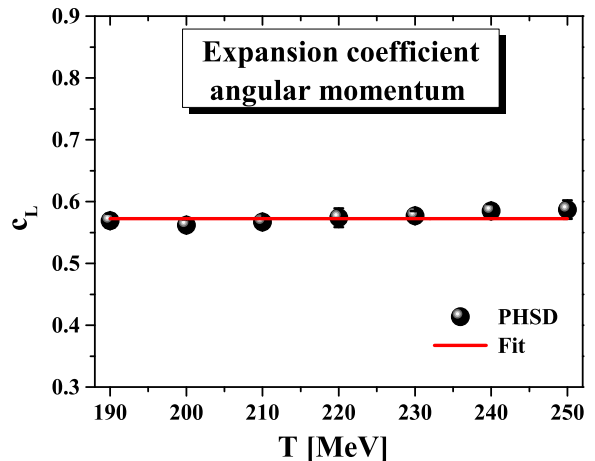


FIG. 14: (Color online) The coefficient  $c_L$  in Eq. (37) for  $\Delta E_{mag,L}$  in case of finite  $\mu_q \leq 100$  MeV as a function of temperature  $T$ .

## IV. SUMMARY

In conclusion, we have evaluated the electric conductivity  $\sigma_0(T, \mu_q)$  of the quark-gluon plasma as a function of temperature  $T$  and quark chemical potential  $\mu_q$  by employing the Parton-Hadron-String Dynamics (PHSD) off-shell transport model in a finite box for the simulation of dynamical partonic systems in equilibrium. The PHSD approach in the partonic sector is based on the lattice QCD equation of state of [1]; accordingly, it describes the QGP entropy density  $s(T)$ , the energy density  $\varepsilon(T)$  and the pressure  $p(T)$  from lQCD [17, 60, 71] very well. Studies of the QCD matter within PHSD have previously given reasonable results also for the shear and bulk viscosities  $\eta$  and  $\zeta$  versus  $T$  [18] and related transport coefficients [59].

In extension of our previous study in Ref. [58] we have found that the electric conductivity shows a simple

scaling with  $\mu_q^2/T^2$  (cf. Eq.(8)) which essentially can be traced back to the variation of the quark+antiquark density  $n_{q+\bar{q}}$  of the system in the Dynamical QuasiParticle Model (DQPM). We recall that PHSD calculations in a fixed box in equilibrium give practically the same results for the equation of state of QCD matter and transport coefficients as the DQPM [17, 18]. In analogy to the ratio of shear viscosity to entropy density  $\eta/s$  we find a clear minimum of the dimensionless ratio  $\sigma_0/T$  in the vicinity of the critical temperature  $T_c$  with values close to more recent lattice QCD calculations [37, 40, 41]. This prediction as well as the explicit dependence on  $\mu_q$  should be controlled by related QCD studies on the lattice. The frequency dependence of the complex electric conductivity  $\sigma(\Omega)$  is found to be well in line with the simple results from the DQPM (11), too.

Furthermore, we have explored the response of the partonic system on a moderate external magnetic field  $eB \leq 0.1$  GeV/fm and studied separately the diamagnetic response from the Lorentz force (1) and the paramagnetic response due to the interaction of the quark spin with the magnetic field in Eq. (13). Within the temperature range investigated ( $170 \text{ MeV} < T < 250 \text{ MeV}$ ) the magnetic moment due to the Lorentz force rises with temperature  $T$  but drops with  $1/B$  providing a constant energy shift due to a coupling to the magnetic field  $\Delta E_{mag,L}(\mu_q) > 0$ . The coupling of the spin to the

$B$ -field gives a paramagnetic contribution which can well be characterized by a magnetic susceptibility  $\chi_S(T, \mu_q)$ . Its contribution to the energy shift of the system is negative and increases with  $B^2$ . According, there is a 'critical' magnetic field  $B_c(T)$  for which the response of the system changes from diamagnetic to paramagnetic. The actual values for  $B_c(T)$  (cf. Fig. 12) demonstrate that the response of the QGP in ultrarelativistic heavy-ion collisions should be diamagnetic since the maximal magnetic fields created in these collisions are smaller than  $B_c(T)$ . As in case of the electric conductivity the dependence of the energy shift  $\Delta E_{mag,L}(\mu_q)$  as well as the magnetic susceptibility  $\chi_S(T, \mu_q)$  show a very similar scaling correction  $\sim \mu_q^2/T^2$  with a coefficient of order 0.5. We close by noting that in the hadronic phase for temperatures below  $T_c$  and  $\mu_q = 0$  the system dominantly consists of pseudoscalar mesons that have no spin and accordingly a low (or vanishing) paramagnetic contribution to the magnetization  $M$  when restricting to the first order in the magnetic field. On the other hand, the charged hadrons see the Lorentz force (1) and build up a diamagnetic contribution.

The authors acknowledge valuable discussions with E. L. Bratkovskaya, V. Konchakovski, O. Linnyk and R. Marty during the course of this study which was supported by the LOEWE center HIC for FAIR.

- 
- [1] Y. Aoki *et al.*, Phys. Lett. B **643**, 46 (2006); S. Borsanyi *et al.*, JHEP **1009**, 073 (2010); JHEP **1011**, 077 (2010); JHEP **1208**, 126 (2012); Phys. Lett. B **370**, 99 (2014).
- [2] P. Petreczky [HotQCD Collaboration], PoS LATTICE **2012**, 069 (2012); AIP Conf. Proc. **1520**, 103 (2013).
- [3] M. Gyulassy and L. D. McLerran, Nucl. Phys. A **750**, 30 (2005); E. V. Shuryak, Nucl. Phys. A **750**, 64 (2005); U. W. Heinz, AIP Conf. Proc. **739**, 163 (2004); A. Peshier and W. Cassing, Phys. Rev. Lett. **94**, 172301 (2005).
- [4] J. Adams *et al.* (STAR Collaboration), Nucl. Phys. A **757**, 102 (2005).
- [5] K. Adcox *et al.* (PHENIX Collaboration), Nucl. Phys. A **757**, 184 (2005).
- [6] I. Arsene *et al.* (BRAHMS Collaboration), Nucl. Phys. A **757**, 1 (2005).
- [7] B. B. Back *et al.* (PHOBOS Collaboration), Nucl. Phys. A **757**, 28 (2005).
- [8] K. Aamodt *et al.* (ALICE Collaboration), Phys. Rev. Lett. **105**, 252302 (2010).
- [9] P. Huovinen *et al.*, Phys. Lett. B **503**, 58 (2001).
- [10] P. F. Kolb, P. Huovinen, U. Heinz, and H. Heiselberg, Phys. Lett. B **500**, 232 (2001).
- [11] D. Teaney, J. Lauret, and E. V. Shuryak, Phys. Rev. Lett. **86**, 4783 (2001).
- [12] T. Hirano and K. Tsuda, Phys. Rev. C **66**, 054905 (2002).
- [13] P. F. Kolb and R. Rapp, Phys. Rev. C **67**, 044903 (2003).
- [14] P. Huovinen, in *Quark-Gluon Plasma 3*, edited by R. C. Hwa and X.-N. Wang (World Scientific, Singapore, 2004); P. F. Kolb and U. W. Heinz, edited by R. C. Hwa and X.-N. Wang (World Scientific, Singapore, 2004).
- [15] H. B. Meyer, Phys. Rev. D **76**, 101701 (2007).
- [16] S. Sakai and A. Nakamura, Pos **LAT2007**, 221 (2007).
- [17] V. Ozvenchuk, O. Linnyk, M. I. Gorenstein, E. L. Bratkovskaya, and W. Cassing, Phys. Rev. C **87**, 024901 (2013).
- [18] V. Ozvenchuk, O. Linnyk, M. I. Gorenstein, E. L. Bratkovskaya, and W. Cassing, Phys. Rev. C **87**, 064903 (2013).
- [19] R. A. Lacey and A. Taranenko, PoS **CFRNC2006**, 021 (2006).
- [20] D. Kharzeev and K. Tuchin, JHEP **09**, 093 (2008).
- [21] F. Karsch, D. Kharzeev, and K. Tuchin, Phys. Lett. B **663**, 217 (2008).
- [22] P. Romatschke and D. T. Son, Phys. Rev. D **80**, 065021 (2009).
- [23] G. D. Moore and O. Saremi, JHEP **09**, 015 (2008).
- [24] C. Sasaki and K. Redlich, Phys. Rev. C **79**, 055207 (2009); Nucl. Phys. A **832**, 62 (2010).
- [25] G. Policastro, D. T. Son, A. O. Starinets, Phys. Rev. Lett. **87**, 081601 (2001); P. K. Kovtun, D. T. Son, A. O. Starinets, Phys. Rev. Lett. **94**, 111601 (2005).
- [26] L.P. Csernai, J.I. Kapusta and L.D. McLerran, Phys. Rev. Lett. **97**, 152303 (2006).
- [27] T. Hirano and M. Gyulassy, Nucl. Phys. A **769**, 71 (2006).
- [28] B. Jacak and P. Steinberg, Phys. Today **53**, 39 (2010).
- [29] P. Romatschke, U. Romatschke, Phys. Rev. Lett. **99**, 172301 (2007).
- [30] H. Song and U. W. Heinz, Phys. Rev. C **77**, 064901 (2008).

- [31] M. Luzum and P. Romatschke, Phys. Rev. C **78**, 034915 (2008).
- [32] B. Schenke, S. Jeon, and C. Gale, Phys. Rev. C **82**, 014903 (2010).
- [33] S. Plumari, A. Puglisi, F. Scardina, and V. Greco, Phys. Rev. C **86**, 054902 (2012).
- [34] S. Mattiello and W. Cassing, Eur. Phys. J. C **70**, 243 (2010).
- [35] Y. Hirono, M. Hongo and T. Hirano, arXiv:1211.1114.
- [36] S. I. Finazzo and J. Noronha, arXiv:1311.6675.
- [37] H.-T. Ding *et al.*, Phys. Rev. D **83**, 034504 (2011); O. Kaczmarek *et al.*, PoS Confinement X, 185 (2012).
- [38] G. Aarts, C. Allton, J. Foley, S. Hands, and S. Kim, Phys. Rev. Lett. **99**, 022002 (2007).
- [39] S. Gupta, Phys. Lett. B **597**, 57 (2004).
- [40] P. V. Buividovich *et al.*, Phys. Rev. Lett. **105**, 132001 (2010).
- [41] B. B. Brandt, A. Francis, H. B. Meyer and H. Wittig, PoS Confinement X, 112 (2012).
- [42] K. Tuchin, Adv. High Energy Phys. **2013**, 490495 (2013)
- [43] D. E. Kharzeev, L. D. McLerran, and H. J. Warringa, Nucl. Phys. A **803**, 227 (2008).
- [44] D. E. Kharzeev, Ann. Phys. (NY) **325**, 205 (2010).
- [45] K. Fukushima, D. E. Kharzeev, and H. J. Warringa, Phys. Rev. D **78**, 074033 (2008).
- [46] D. Kharzeev and A. Zhitnitsky, Nucl. Phys. A **797**, 67 (2007).
- [47] D. E. Kharzeev and H. J. Warringa, Phys. Rev. D **80**, 034028 (2009).
- [48] V. Skokov, A. Illarionov, and V. Toneev, Int. J. Mod. Phys. A **24**, 5925 (2009).
- [49] G.S. Bali, F. Bruckmann, G. Endrodi, Z. Fodor, S.D. Katz, S. Krieg, A. Schäfer, and K.K. Szabo, JHEP **1202**, 044 (2012).
- [50] G. S. Bali, F. Bruckmann, M. Constantinou, M. Costa, G. Endrodi, S. D. Katz, H. Panagopoulos and A. Schäfer, Phys. Rev. D **86**, 094512 (2012).
- [51] G.S. Bali, F. Bruckmann, G. Endrodi, F. Gruber, and A. Schäfer, JHEP **1304**, 130 (2013).
- [52] G.S. Bali, F. Bruckmann, G. Endrodi, and A. Schäfer, e-Print: arXiv:1310.8145
- [53] V. Voronyuk, V. D. Toneev, W. Cassing, E. L. Bratkovskaya, V. P. Konchakovski, and S. A. Voloshin, Phys. Rev. C **83**, 054911 (2011).
- [54] V.D. Toneev, V.P. Konchakovski, V. Voronyuk, E.L. Bratkovskaya, and W. Cassing, Phys. Rev. C **86**, 064907 (2012).
- [55] H. van Hees, C. Gale, and R. Rapp, Phys. Rev. C **84**, 054906 (2011).
- [56] C. Shen, U. Heinz, J.-F. Paquet, and C. Gale, e-Print: arXiv:1308.2440.
- [57] O. Linnyk, V.P. Konchakovski, W. Cassing, E.L. Bratkovskaya, Phys. Rev. C **88**, 034904 (2013).
- [58] W. Cassing, O. Linnyk, T. Steinert, and V. Ozvenchuk, Phys. Rev. Lett. **110**, 182301 (2013).
- [59] R. Marty, E. Bratkovskaya, W. Cassing, J. Aichelin, and H. Berrehrhah, Phys. Rev. C **88**, 045204 (2013).
- [60] W. Cassing and E. L. Bratkovskaya, Nucl. Phys. A **831**, 215 (2009); Phys. Rev. C **78**, 034919 (2008).
- [61] L. P. Kadanoff and G. Baym, *Quantum Statistical Mechanics*, (Benjamin, New York, 1962).
- [62] S. Juchem, W. Cassing, and C. Greiner, Phys. Rev. D **69**, 025006 (2004); Nucl. Phys. A **743**, 92 (2004).
- [63] W. Cassing and E. L. Bratkovskaya, Phys. Rept. **308**, 65 (1999).
- [64] E. L. Bratkovskaya and W. Cassing, Nucl. Phys. A **619**, 413 (1997).
- [65] W. Cassing, Nucl. Phys. A **700**, 618 (2002).
- [66] E. L. Bratkovskaya, S. Soff, H. Stöcker, M. van Leeuwen, and W. Cassing, Phys. Rev. Lett. **92**, 032302 (2004).
- [67] W. Cassing, V. Metag, U. Mosel, and K. Niita, Phys. Rep. **188**, 363 (1990).
- [68] W. Cassing, Nucl. Phys. A **795**, 70 (2007).
- [69] W. Cassing, Nucl. Phys. A **791**, 365 (2007).
- [70] A. Peshier, Phys. Rev. D **70**, 034016 (2004); J. Phys. G **31**, S371 (2005).
- [71] E. L. Bratkovskaya, W. Cassing, V. P. Konchakovski, and O. Linnyk, Nucl. Phys. A **856**, 162 (2011).
- [72] W. Cassing, Eur. Phys. J. ST **168**, 3 (2009).
- [73] A. Amato, G. Aarts, C. Allton, P. Giudice, S. Hands, and J.-I. Skullerud, Phys. Rev. Lett. **111**, 172001 (2013).
- [74] O. Linnyk, W. Cassing, J. Manninen, E.L. Bratkovskaya, P.B. Gossiaux, J. Aichelin, T. Song, C.M. Ko, Phys. Rev. C **87**, 014905 (2013).